



## Article

# Characterizing the Accelerated Global Carbon Emissions from Forest Loss during 1985–2020 Using Fine-Resolution Remote Sensing Datasets

Wendi Liu <sup>1,2,3</sup>, Xiao Zhang <sup>1,2</sup>, Hong Xu <sup>4</sup>, Tingting Zhao <sup>1,2,5</sup>, Jinqing Wang <sup>1,2,3</sup>, Zhehua Li <sup>1,2,3</sup> and Liangyun Liu <sup>1,2,3,\*</sup>

- <sup>1</sup> Key Laboratory of Digital Earth Science, Aerospace Information Research Institute, Chinese Academy of Sciences, Beijing 100094, China; liuwendi20@mails.ucas.ac.cn (W.L.); zhangxiao@radi.ac.cn (X.Z.); 21210061042@stu.xust.edu.cn (T.Z.); wangjinqing21@mails.ucas.ac.cn (J.W.); lizhehua22@mails.ucas.ac.cn (Z.L.)
- <sup>2</sup> International Research Center of Big Data for Sustainable Development Goals, Beijing 100094, China
- <sup>3</sup> University of Chinese Academy of Sciences, Beijing 100049, China
- <sup>4</sup> The High-Tech Research & Development Center (HTRDC) of the Ministry of Science & Technology, Beijing 100044, China; xuhong@nsfc.gov.cn
- <sup>5</sup> College of Geomatics, Xi'an University of Science and Technology, Xi'an 710054, China
- \* Correspondence: liuly@radi.ac.cn

**Abstract:** Previous studies on global carbon emissions from forest loss have been marked by great discrepancies due to uncertainties regarding the lost area and the densities of different carbon pools. In this study, we employed a new global 30 m land cover dynamic dataset (GLC\_FCS30D) to improve the assessment of forest loss areas; then, we combined multi-sourced carbon stock products to enhance the information on carbon density. Afterwards, we estimated the global carbon emissions from forest loss over the period of 1985–2020 based on the method recommended by the Intergovernmental Panel on Climate Change Guidelines (IPCC). The results indicate that global forest loss continued to accelerate over the past 35 years, totaling about 582.17 Mha and leading to total committed carbon emissions of  $35.22 \pm 9.38$  PgC. Tropical zones dominated global carbon emissions (~2/3) due to their higher carbon density and greater forest loss. Furthermore, global emissions more than doubled in the period of 2015–2020 ( $1.77 \pm 0.44$  PgC/yr) compared to those in 1985–2000 ( $0.69 \pm 0.21$  PgC/yr). Notably, the forest loss at high altitudes (i.e., above 1000 m) more than tripled in mountainous regions, resulting in more pronounced carbon emissions in these areas. Therefore, the accelerating trend of global carbon emissions from forest loss indicates that great challenges still remain for achieving the COP 26 Declaration to halt forest loss by 2030.

**Keywords:** forest loss; carbon emissions; land cover; tropical rainforest; mountainous forest



**Citation:** Liu, W.; Zhang, X.; Xu, H.; Zhao, T.; Wang, J.; Li, Z.; Liu, L. Characterizing the Accelerated Global Carbon Emissions from Forest Loss during 1985–2020 Using Fine-Resolution Remote Sensing Datasets. *Remote Sens.* **2024**, *16*, 978. <https://doi.org/10.3390/rs16060978>

Academic Editor: Hubert Hasenauer

Received: 23 January 2024

Revised: 28 February 2024

Accepted: 5 March 2024

Published: 11 March 2024



**Copyright:** © 2024 by the authors. Licensee MDPI, Basel, Switzerland. This article is an open access article distributed under the terms and conditions of the Creative Commons Attribution (CC BY) license (<https://creativecommons.org/licenses/by/4.0/>).

## 1. Introduction

Forests cover nearly one-third of the world's land, and they occupy 77% of global vegetation carbon stocks, about 662 PgC [1]. Forest loss is the primary form of global land-cover change [2], which can re-release most of the carbon that has been fixed by photosynthesis into the atmosphere and substantially reduce the carbon sink capacity of terrestrial ecosystems [3,4]. The resulting carbon emissions from global forest loss have been an important driver of rising atmospheric CO<sub>2</sub> concentrations and accelerating global warming [5]. Over the period of 1850–2000, forest loss has contributed about 30% of anthropogenic carbon emissions [6], and the emissions in some hot-spot regions have not slowed as expected in the 21st century [7,8].

Many studies have advocated the application of remote sensing-based datasets to quantify the global carbon emissions from forest loss [9–11]. This is because they are able to provide spatially explicit information on forest loss and carbon density in a globally

consistent way, which is key to estimating carbon emissions from forest loss [9,12], and they can enrich information in region/countries with limited capacity to conduct detailed inventories. Nevertheless, a recent study evaluated the potential of remote sensing-based datasets to support the Global Stocktake Process, known as the ESA-CCI RECCAP2 pilot project [13]. The researchers concluded that these current coarse-resolution maps were insufficient for accurately estimating carbon emissions from global forest loss (e.g., HYDE [14], LUH2 [15], FAOSTAT [16]). They emphasized the need to use fine-resolution (10–30 m) LULCC and biomass remote sensing datasets, as a result of their ability to enhance forest loss information and reduce the uncertainty and bias in the density values of various carbon pools [17].

In terms of the forest loss area, due to large amounts of fragmented forest [18–20] and the increasing small-scale forest loss [21,22], coarse-resolution maps are no longer suitable for capturing forest loss. They tend to attribute the subgrid-scale forest loss to forest degradation in heterogeneous areas [12]. In contrast, fine-resolution maps can represent the spatiotemporal patterns of forest loss more accurately. However, to our knowledge, these currently available fine-resolution remote sensing-based products are not adequate for accessing spatiotemporal information on global forest loss for various reasons: FROM-GLC [23] has a short time span, covering only 2015 and 2017; GlobeLand30 [24] suffers from geometric registration issues stemming from its diverse satellite data sources, making it not suitable for assessing the gross forest loss on fine scales, such as 30 m, when comparing maps between periods [25]; GLanCE [26] lacks information on several crucial land use categories (e.g., cropland) that have great impacts on forest loss because of its coarse classification system, which includes only water, ice/snow, developed, barren, trees, shrubs, and herbaceous; and the Global Forest Cover Change (GFCC) [27] dataset is produced using inconsistent algorithms before and after 2010, which makes it difficult to establish the forest loss trend by making comparisons between periods [28]. Recently, a new global 30 m land cover product named GLC\_FCS30D was generated by coupling continuous change detection and time series Landsat imagery; it contains 35 land cover types and spans the period of 1985–2020 [29,30]. Considering the advantages of a leading mapping strategy, fine classification system, and long time span, it is more suitable than these above products for evaluating the spatiotemporal dynamics and drivers of global forest loss during 1985–2020.

Regarding information on carbon density, biomass and soil are the two main carbon pools, as the carbon stocks of dead wood and litter are usually derived from biomass [31,32]. For the biomass carbon pool, current studies often obtain carbon density through products based on a single type of data, such as light detection and ranging (LiDAR), synthetic aperture radar (SAR), and field inventories [33–35]. These products have different limitations due to the constraints of each data source, such as high uncertainty in regions with above-ground biomass (AGB)  $> 250 \text{ Mg}\cdot\text{ha}^{-1}$  [35], poor spatial representation in eastern Asia [33], and typically failing to accurately describe the global distribution of biomass. Nevertheless, many researchers have indicated that the integration of products from multiple sources allows for more representative information on biomass, and this practice is now widely used [36–38]. For the soil carbon pool, organic carbon is the primary component and is most commonly considered in carbon emissions resulting from land use change [31]. Given that the soil organic carbon (SOC) pool can be easily affected by various factors (e.g., temperature, precipitation, and land cover change) and tends to vary significantly over time [39], dynamic SOC information is crucial for accurately estimating the carbon emissions between different periods. Instead of the widely used static maps [40,41], Xie et al. [42] created a time series SOC dataset covering 1981–2018, providing strong support for addressing this need.

Therefore, the objectives of our study were (1) to derive the amount of global forest loss and resulting carbon emissions during 1985–2020 based on a novel fine-resolution land cover dataset and multi-sourced carbon stock products; and (2) to clarify the spatial distribution and temporal dynamics of global carbon emissions.

## 2. Materials and Methods

### 2.1. Materials

#### 2.1.1. Global Land Cover Dataset

The GLC\_FCS30D dataset was developed by employing all available Landsat imagery on the Google Earth Engine platform in a new land cover mapping scheme that couples continuous change detection and dynamic updates [29,43–45]. It has a fine classification system comprising 35 land cover types and provides global land cover information at a 30 m resolution throughout this study period. The assessed results from a global validation dataset indicated that it achieved an overall accuracy of 80.88% ( $\pm 0.27\%$ ) for the year 2020 for ten major land cover types, and two regional time series validation datasets also demonstrated its strong performance in time series accuracy, achieving a mean overall accuracy of 79.50% ( $\pm 0.50\%$ ) across the contiguous United States and 81.91% ( $\pm 0.09\%$ ) across the European Union. However, owing to the sparse or even absent satellite observations before the year 2000 (only Landsat 5 acquired single-satellite data) [46], the GLC\_FCS30D is available at five-year intervals during 1985–2000, and its credibility for this period still needs to be improved; additionally, false detection of changes at the interannual scale can occur due to various factors, such as fluctuations in climatic conditions [29]. Consequently, we finally chose to acquire information on global forest loss for five periods: 1985–2000, 2000–2005, 2005–2010, 2010–2015, and 2015–2020.

#### 2.1.2. Global Biomass Datasets

Considering the importance of different data sources in accurately obtaining biomass information and the great spatial heterogeneity of carbon density, this study utilized five global biomass products from various sources with fine resolution; these are hereafter referred to as “GFW” [28], “Gibbs and Ruesch” [34], “GLASS” [47], “GlobBiomass” [35], and “GEDI-L4B” [48] (detailed information is shown in Table 1). Specifically, GFW was created by integrating ground measurements, the spaceborne LiDAR observations from the Geoscience Laser Altimeter System (GLAS), and variables derived from satellite products. Gibbs and Ruesch was generated by remapping the default values of regional biomass stocks provided by the IPCC Guidelines to grid level using a GIS-based approach. GLASS was produced by modeling the relationships among regional LiDAR-based AGB products, a suite of high-level satellite products (gross primary production, leaf area index, etc.), and other auxiliary datasets. GlobBiomass was generated by using multiple satellite observations of SAR backscatter to estimate the density of growing wood volume, from which AGB was then computed. GEDI-L4B was created primarily through a closed-form statistical estimation approach called hybrid inference, which used all the GEDI (Global Ecosystem Dynamics Investigation) Level 4A footprint AGB predictions in each 1 km grid to estimate the mean AGB density for that grid.

**Table 1.** Detailed information of biomass datasets used in this study.

Dataset Name	Data source	Spatial Resolution	Year	Carbon Pools
GFW	① Ground-measured biomass plots ② GLAS-based observations ③ Variables of Landsat imagery and several vegetation indexes such as NDVI, NDII, etc.	30 m	2000	AGB
Gibbs and Ruesch	Field measurements	1 km	2000	AGB, BGB
GLASS	① LiDAR-based AGB datasets ② High-level satellite products ③ Auxiliary datasets, including GLAS-based canopy height	1 km	2005	AGB
GlobBiomass	Observations of SAR backscatter from ALOS PALSAR and Envisat ASAR	100 m	2010	AGB

Table 1. Cont.

Dataset Name	Data source	Spatial Resolution	Year	Carbon Pools
GEDI-LAB	① GEDI-based observations ② Field measurements ③ Simulated GEDI waveforms	1 km	2020	AGB

Note: belowground biomass (BGB).

### 2.1.3. Global SOC Dataset

A long time series SOC dataset [42] was selected in this study to capture the dynamics of organic carbon in topsoil (0–30 cm), a depth defined by the Tier 1 method in IPCC Guidelines [31]. It was created by combining the process-based RothC model and a geographically weighted regression kriging method, achieving a root-mean-squared accuracy of 27.76 tC/ha. It includes the annual SOC stocks from 1981 to 2018, and it spans all latitudes from 90°N to 90°S and longitudes from 180°W to 180°E, with a spatial resolution of about 5 km.

### 2.1.4. Other Data

The third version of the Advanced Spaceborne Thermal Emission and Reflection Radiometer Global Digital Elevation Model (ASTER GDEM) was used to supply elevation information [49,50]; this product has a 30 m spatial resolution with great coverage between 83°N and 83°S. The Global Mountain Biodiversity Assessment (GMBA) inventory data V1.2 were chosen to obtain the distribution of mountainous regions [51]. Administrative boundary data and a global forest ecological zone map [52] were used to provide boundary information on countries and ecological zones.

## 2.2. Methods

Figure 1 illustrates the flowchart of the proposed method for estimating global carbon emissions from forest loss and quantifying their uncertainty. It comprises four main steps: First, we divided the global land into approximately 2.4 million  $0.1 \times 0.1^\circ$  grids; within each grid, we established the lookup table (LUT) of carbon density for five carbon pools in different types of forests, including AGB, BGB, SOC, dead wood, and litter [31]. Second, by overlaying land cover maps from different periods, we calculated the area that has been converted to other land cover categories for different types of forests within each  $0.1^\circ$  grid. Third, we assessed the carbon emissions within each  $0.1^\circ$  grid by combining the forest conversion area with the LUT of carbon density, and we quantified the uncertainty of carbon emissions by utilizing the five biomass products. Finally, we employed the GMBA and the ASTER GDEM V3 to clarify the carbon emissions in mountainous regions and investigate their trends regarding altitude.

### 2.2.1. Establishing the LUT of Carbon Density

Considering the fact that forest carbon density has great spatial heterogeneity, i.e., it varies noticeably across regions and forest types, as well as the spatial resolution variations among different products (ranging from 30 m to 1 km), we chose to establish the LUT of carbon density for different forest types at each  $0.1^\circ$  grid [53]. For the carbon density of AGB, BGB, dead wood, and litter in the LUT, we used the combination of five global biomass products, which helps reduce bias and quantify the uncertainty. Taking the calculation of AGB carbon (AGBC) density in the LUT as an example, we first derived the AGBC maps from these five biomass products, assuming that the carbon fraction of biomass was 0.5 [54]. Then, we resampled all five AGBC maps to 30 m spatial resolution by using the nearest-neighbor method to match the land cover dataset. For each resampled AGBC map, we overlaid it with the land cover map at the corresponding time (Table 1) to obtain the AGBC information of all forest pixels with AGBC values greater than 0; then, we calculated the mean AGBC value for different types of forests within each  $0.1^\circ$  grid. Finally, we got five

mean AGBC values from these five AGBC maps for each forest type within the  $0.1^\circ$  grid; and following the approach of Feng et al. [55] and Friedlingstein et al. [5], we took the mean and standard deviation value of them as the AGBC density and its uncertainty for each forest type in the LUT, respectively. The same process was carried out for calculating the carbon density of BGB, dead wood, and litter in the LUT: for biomass products containing only AGB, the BGB was calculated based on the shoot-to-root ratio according to the IPCC Guidelines [31]; and the carbon stocks of dead wood and litter pools were determined based on their relationships with AGB pool [32], with detailed information shown in Table A2. In addition, for the SOC density in the LUT, we chose the average of the SOC density for each five-year period as the basic data, and we conducted the same calculations as described above to generate a dynamic LUT; but we did not quantify the uncertainty, since only one SOC product was used in this study. These were calculated in each  $0.1^\circ$  grid as follows:

$$\text{mean}_{i,j,k} = \frac{1}{n} \sum_{p=1}^{p=n} \text{carbon}_{i,j,k}^p \quad (1)$$

$$\text{LUT\_mean}_{i,j,k} = \frac{1}{5} \sum_{i=1}^{i=5} \text{mean}_{i,j,k} \quad (2)$$

$$\text{LUT\_uncertainty}_{i,j,k} = \sqrt{\frac{1}{5} \sum_{i=1}^{i=5} (\text{mean}_{i,j,k} - \text{LUT\_mean}_{i,j,k})^2} \quad (3)$$

where  $\text{carbon}_{i,j,k}^p$  is the carbon value of the  $p$ th pixel belonging to the  $i$ th biomass product, forest type  $j$ , and carbon pool type  $k$  within each  $0.1^\circ$  grid.  $\text{LUT\_mean}_{i,j,k}$  and  $\text{LUT\_uncertainty}_{i,j,k}$  represent the carbon density value and its uncertainty for forest type  $j$  and carbon pool type  $k$  in the LUT, respectively.

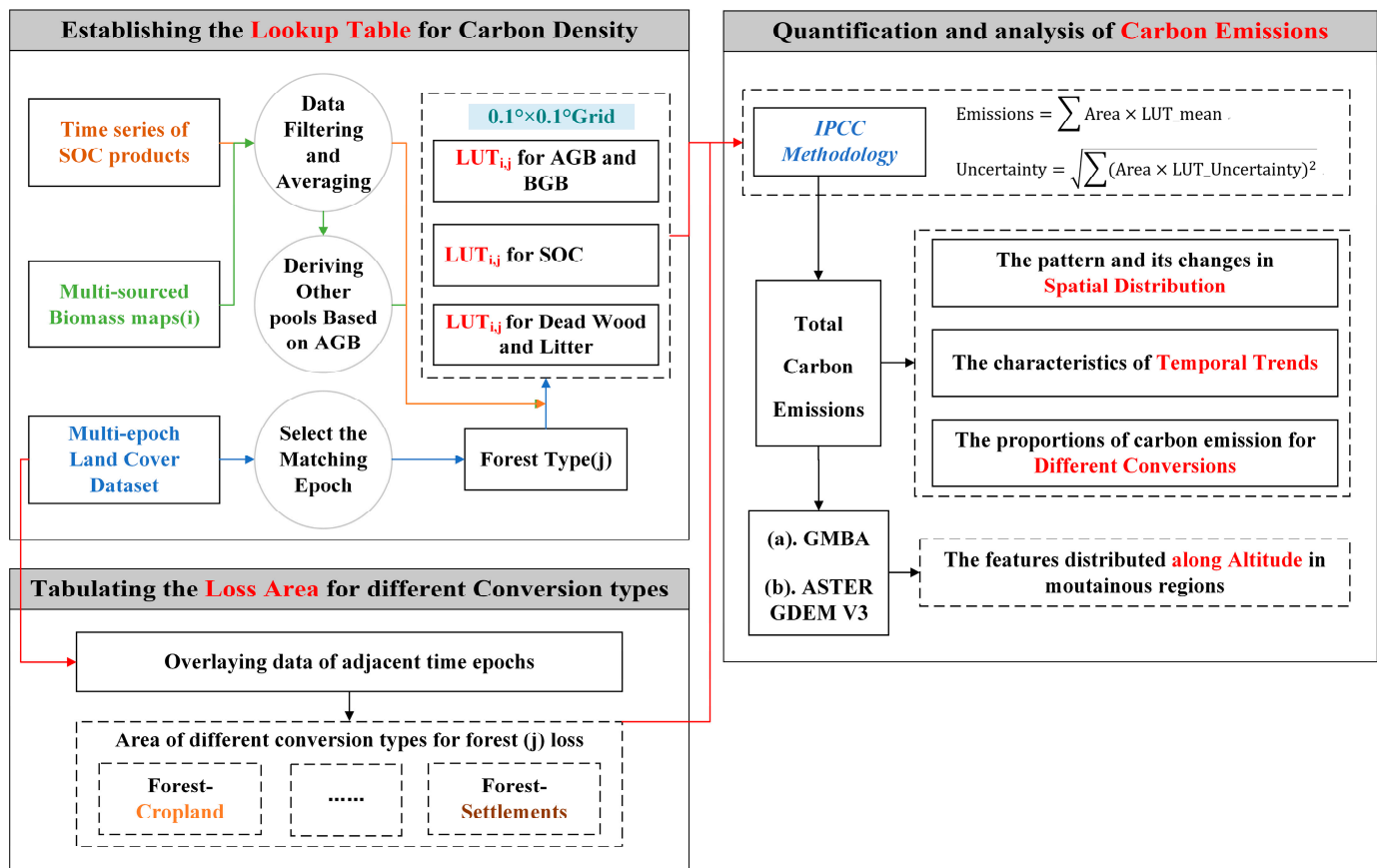


Figure 1. Flowchart for quantifying and analyzing global carbon emissions from forest loss.

### 2.2.2. Assessing the Area of Forest Converted to other Land Cover Categories

Forest loss is defined as a stand-replacement disturbance or the complete removal of the tree cover canopy [27]. This can be presented as the transition of land cover type from forest to non-forest in GLC\_FCS30D. By comparing the land cover products in each study period, we tabulated the area that was converted to other land cover categories for different types of forests within each 0.1° grid. Further, to better clarify the varied impacts of different conversion types (e.g., forest converted to cropland or settlement) on carbon emissions, we adopted the classification system used in the IPCC Guidelines and reclassified the 35 land cover types into six land use categories (cropland, forest land, grassland, wetlands, settlements, and other land); the specific relationships are shown in Table A1.

### 2.2.3. Quantifying Carbon Emissions Due to Forest Loss and Associated Uncertainties

We followed the definition of committed emissions and attributed the carbon emissions to the period in which forest loss occurred [56]. Moreover, we only focused on the carbon emissions during forest loss, without considering the variations in carbon stock in different land cover types after forest loss. Specifically, we assumed the complete loss of all carbon pools except the SOC [54], and we determined the percentages of SOC loss for different conversion types [57,58]; details about the proportions of loss are shown in Table A1. The carbon emissions and their uncertainty within 0.1° grid were calculated as follows:

$$\text{Emission} = \sum_{j,c} \text{Area}_{j,c} \times (\text{LUT\_mean}_{j,k=\text{soc}} \times \text{percent}_c + \sum_k \text{LUT\_mean}_{j,k \neq \text{soc}}) \quad (4)$$

$$\text{Uncertainty} = \sqrt{\sum_{j,c} \left( \text{Area}_{j,c} \times \sqrt{\sum_k (\text{LUT\_uncertainty}_{j,k \neq \text{soc}})^2} \right)^2} \quad (5)$$

where  $j, c$ , and  $k$  represent the forest type, conversion type, and carbon pool type, respectively;  $\text{Area}_{j,c}$  is the forest loss area;  $\text{LUT\_mean}_{j,k=\text{soc}}$  is the SOC density;  $\text{LUT\_mean}_{j,k \neq \text{soc}}$  and  $\text{LUT\_uncertainty}_{j,k \neq \text{soc}}$  are the carbon density and its uncertainty of carbon pool type that belongs to AGBC, BGBC, dead wood, and litter, respectively;  $\text{percent}_c$  is the percentage of SOC loss.

### 2.2.4. Determining the Variation in Carbon Emissions with Altitude in Mountainous Regions

Since the increased intensity of human activities at high altitudes leads to great forest loss [59,60], we employed the GMBA V1.2 to present the carbon emissions in mountainous regions; then, we combined the ASTER GDEM to investigate the trend in resulting emissions with altitude. Considering the elevation accuracy of the DEM product [61], as well as the computational efficiency, we chose 10 m as the interval to calculate the carbon emissions at different altitudes.

$$\text{Emissions}_m = \text{Emissions}_{\text{all}} \bigcup \text{GMBA} \quad (6)$$

$$\text{Emissions}_n^{n+10} = \text{Emissions}_m \bigcup \text{DEM}_n^{n+10} \quad (7)$$

where  $\text{Emissions}_{\text{all}}$  and  $\text{Emissions}_m$  represent global carbon emissions from forest loss occurring in global and mountainous regions, respectively;  $n$  is the serial number of altitudes with intervals of 10 m; and  $\text{Emissions}_n^{n+10}$  represents carbon emissions in mountainous regions whose altitude belong to intervals of  $[n, n + 10]$  m. The uncertainty was calculated using Equation (5).

### 3. Results

#### 3.1. Characteristics of Global Forest Loss over the Past 35 Years

A large amount of forest loss, about 582.17 Mha, occurred during 1985–2020. This was mainly in South America, Asia, Africa, and North America, which accounted for 24.20%, 23.38%, 19.83%, and 18.19% of the total, respectively (Figure 2). Regarding the spatial distribution, most of the forest loss over the past 35 years has taken place in the tropical regions of the Southern Hemisphere, characterized by the Amazon Basin, Southeast Asia, and the Congo Basin, as well as in the temperate regions of the Northern Hemisphere, exemplified by the Gulf Rim of Mexico in North America, and the boreal regions, represented by Russia and Canada (Figure 2).

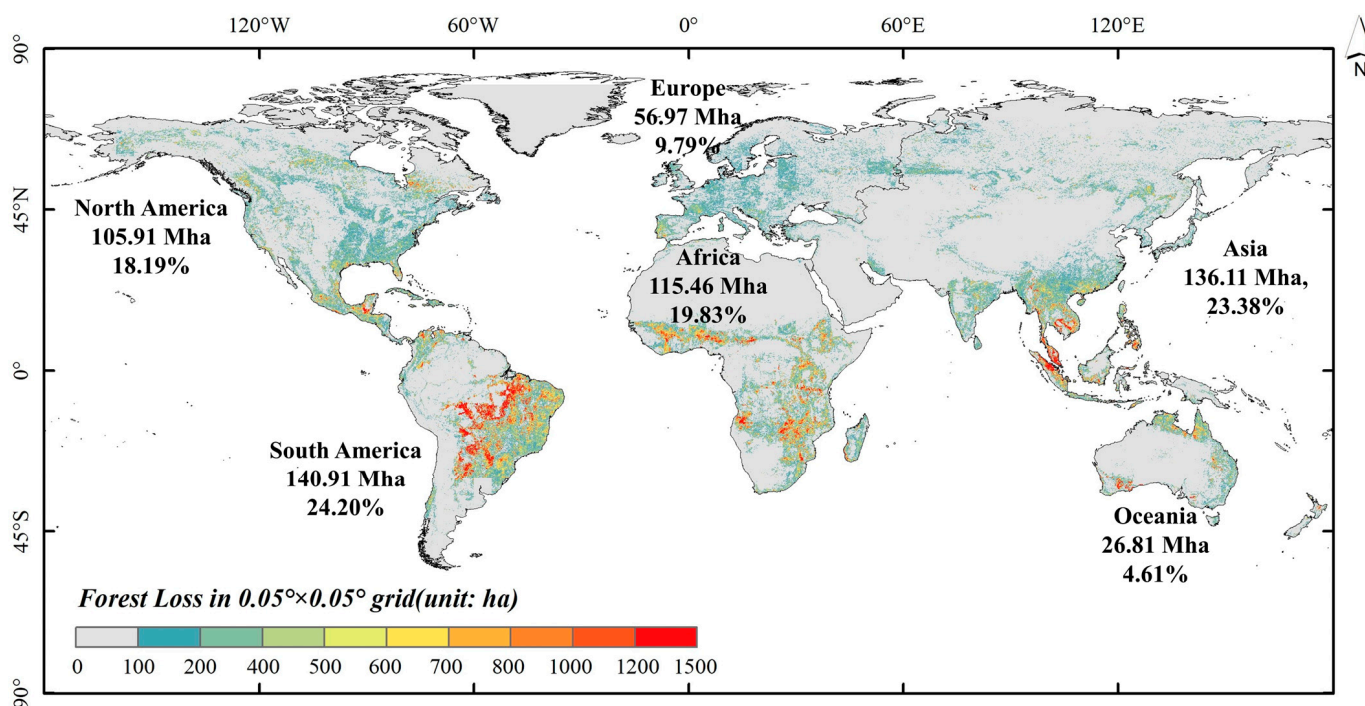


**Figure 2.** Spatial distribution and continent-wise proportions of total forest loss during 1985–2020.

The rate of global forest loss continued to accelerate during this period, with all continents showing obviously increasing trends except for Oceania (Figure 3a). Specifically, Africa and Asia had the top-two rises in forest loss rates, with similar increases of 4.66 and 4.32 Mha/yr, respectively. The former only saw the most rapid increase across continents after 2010, and the latter showed a continuous increase. The forest loss rate in South America returned to an increasing trend after a brief decline during 2005–2010, while in North America, it kept growing. As for specific ecological zones, tropical zones such as moist deciduous forest and rainforest still dominated the growth in the global forest loss area, and there were also obvious increases in other zones outside tropical areas such as boreal coniferous forest and temperate continental forest (Figure 3b).

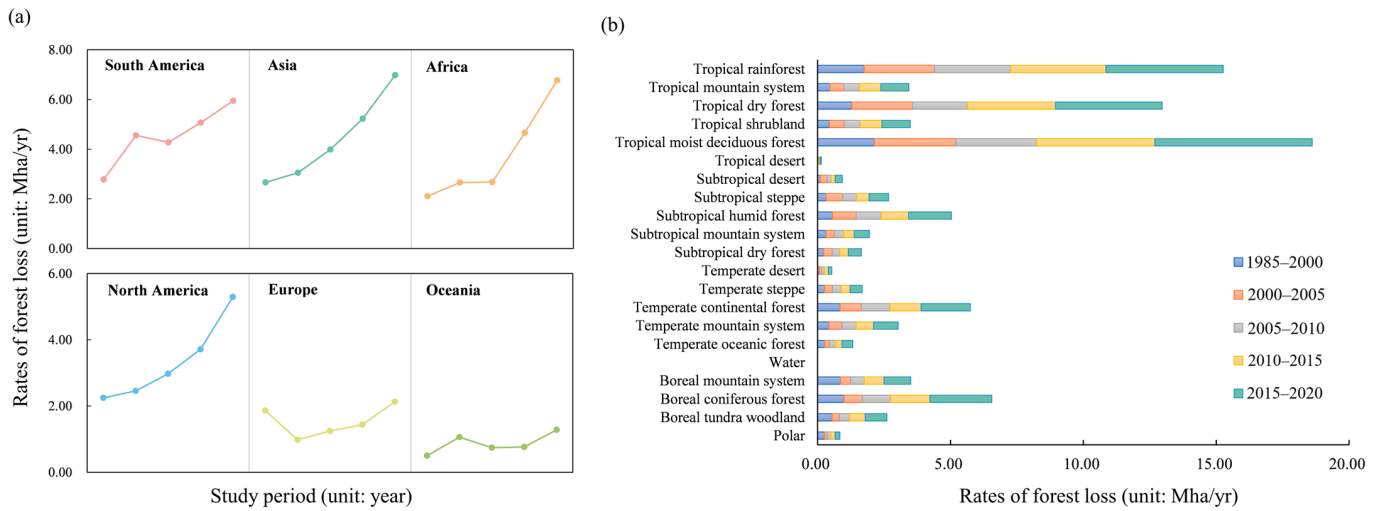


**Figure 3.** Rates of forest loss in different (a) continents and (b) ecological zones. Note: the dots in Figure 3a represent study periods, from left to right, 1985–2000, 2000–2005, 2005–2010, 2010–2015, and 2015–2020.

### 3.2. Patterns of Global Carbon Emissions during the Period 1985–2020

#### 3.2.1. Spatial Distribution of Global Carbon Emissions

The total carbon emissions from global forest loss in 1985–2020 were  $35.22 \pm 9.38$  PgC, and their spatial distribution is illustrated in Figure 4. In general, the carbon emissions notably occurred within three tropical rainforest regions: the Amazon Basin, Southeast Asia, and the Congo Basin. Specifically, the regions with the highest emission densities were located in the Malay Peninsula and Sumatra in Southeast Asia, and the famous “arc of deforestation” of South America; the carbon emissions near the Congo Basin were characterized by a widespread distribution. There were also huge areas of relatively low emission intensity at high latitudes, such as in boreal countries like Russia and Canada.

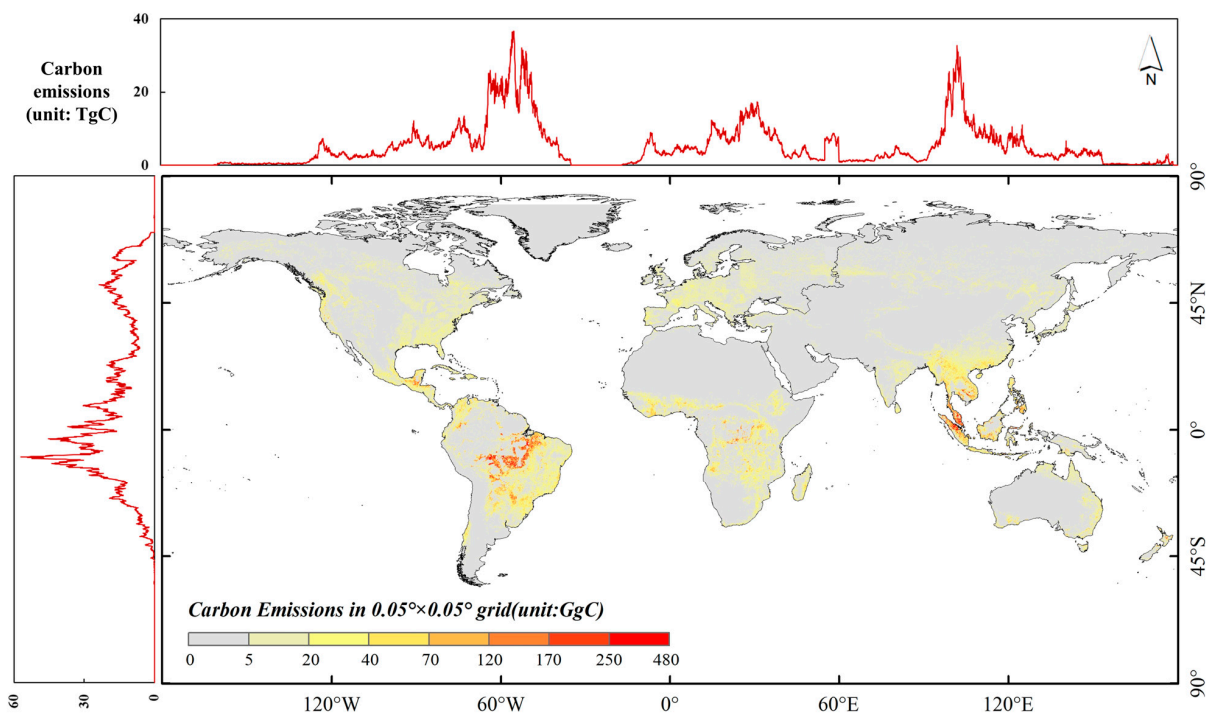


**Figure 4.** Spatial patterns of total global carbon emissions from forest loss between 1985 and 2020.

The distribution of the total carbon emissions along the latitude and longitude directions was also assessed, and the results are shown in Figure 4. It can be seen that the distribution of carbon emissions in the Western Hemisphere was concentrated between 50°W and 65°W, accounting for approximately 40% of the total emissions in this hemisphere. Carbon emissions in the Eastern Hemisphere were higher near 30°E and 100°E. In terms of latitude, emissions were clearly concentrated at low latitudes, mainly between 20°S and 15°N, accounting for about 50% of global emissions. There was also a small peak of carbon emissions at high latitudes near 50°N in the Northern Hemisphere.

By counting carbon emissions on a continental scale, we found that South America, Asia, and Africa were the dominant regions, accounting for about 76% of global emissions. Specifically, South America ranked first, with  $11.13 \pm 3.81$  PgC over the 35-year period. This was followed by Asia ( $10.56 \pm 3.19$  PgC), Africa ( $5.22 \pm 1.41$  PgC), and North America ( $4.83 \pm 1.06$  PgC). Europe and Oceania had much lower emissions, totaling  $2.30 \pm 0.70$  PgC and  $1.18 \pm 0.21$  PgC, respectively.

We further analyzed the changes in the spatial distribution of carbon emissions from forest loss, mainly in these three tropical rainforest regions (the Amazon Basin, Southeast Asia, and the Congo Basin), considering their dominant roles in global carbon emissions. The results showed that carbon emissions in the famous “arc of deforestation” have declined notably, while an obvious increase has occurred in the adjacent northern areas; this indicates that regions with the highest emissions in Brazil have gradually moved northward. In addition, countries in the northern Amazon Basin, such as Colombia and Venezuela, also experienced a great increase in carbon emissions (Figure 5a). Regions in Southeast Asia have all seen rapid growth in carbon emissions, most notably in the southern island of Sumatra, which has come to be the region with the largest emissions. There was also a clear increase in carbon emissions in Kalimantan Island, the Philippines, and countries in the Central South Peninsula (Figure 5b). In the Congo Basin, carbon emissions have continued to be concentrated in the Democratic Republic of the Congo, Angola, Tanzania, and Zambia, with all four countries showing a large growth in emissions. It is worth noting that increasingly dramatic carbon emissions occurred in the northwestern and central regions of the Democratic Republic of the Congo over the past 35 years (Figure 5c).

### 3.2.2. Temporal Trends in Global Carbon Emissions

Global carbon emissions have been accelerating over the past 35 years, more than doubling from  $0.69 \pm 0.21$  PgC/yr in 1985–2000 to  $1.77 \pm 0.44$  PgC/yr in 2015–2020 (Figure 6a). The loss of AGB dominated global carbon emissions throughout the whole study period, accounting for 63.37% ( $22.32 \pm 6.93$  PgC) of the total; BGB, SOC, dead wood, and litter pools accounted for only 19.12% ( $6.73 \pm 1.99$  PgC), 13.27% ( $4.67$  PgC), 2.98% ( $1.05 \pm 0.35$  PgC), and 1.26% ( $0.45 \pm 0.13$  PgC), respectively (Figure 6a). Furthermore, when merging these 21 ecological zones into 4 climate zones (tropical, subtropical, temperate, and boreal; see Table A2), we concluded that the tropical zones dominated the global carbon emissions, accounting for 64.79%; this was followed by the temperate, subtropical, and boreal zones, with 13.97%, 11.26%, and 9.98%, respectively (Figure 6b). All of these also experienced great increases in their carbon emissions: in the tropical and subtropical zones, the emissions almost tripled, increasing from  $402.54 \pm 132.95$  to  $1160.93 \pm 317.16$  TgC/yr and from  $75.08 \pm 16.81$  to  $205.88 \pm 36.00$  TgC/yr, respectively; in temperate zones, the emissions showed stability from 1985 to 2005 but subsequently more than doubled, growing from  $110.35 \pm 31.76$  TgC/yr to  $238.63 \pm 69.01$  TgC/yr; and in boreal zones, the emissions declined between 1985 and 2005, after which they more than doubled, increasing from  $97.75 \pm 38.23$  to  $168.91 \pm 68.11$  TgC/yr.

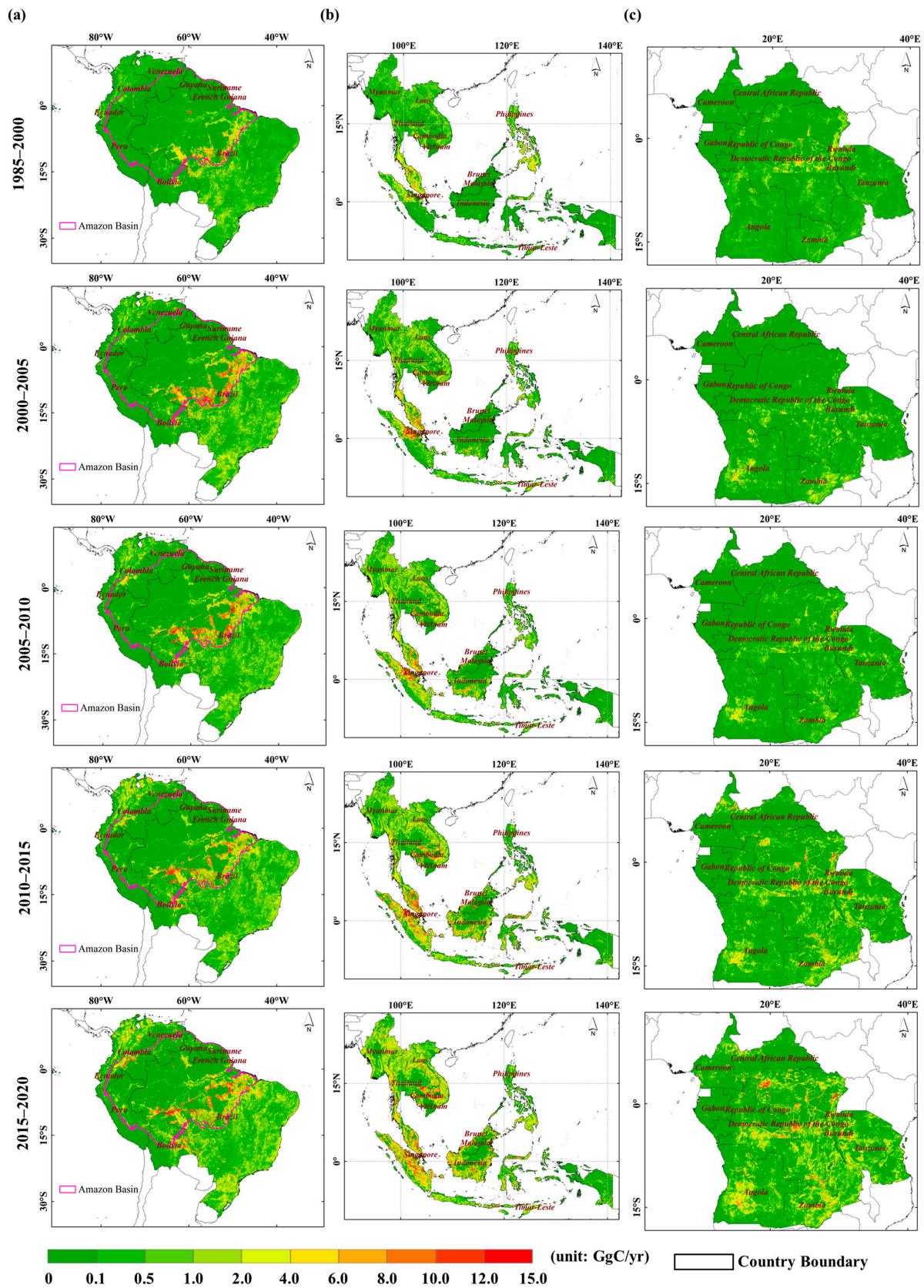
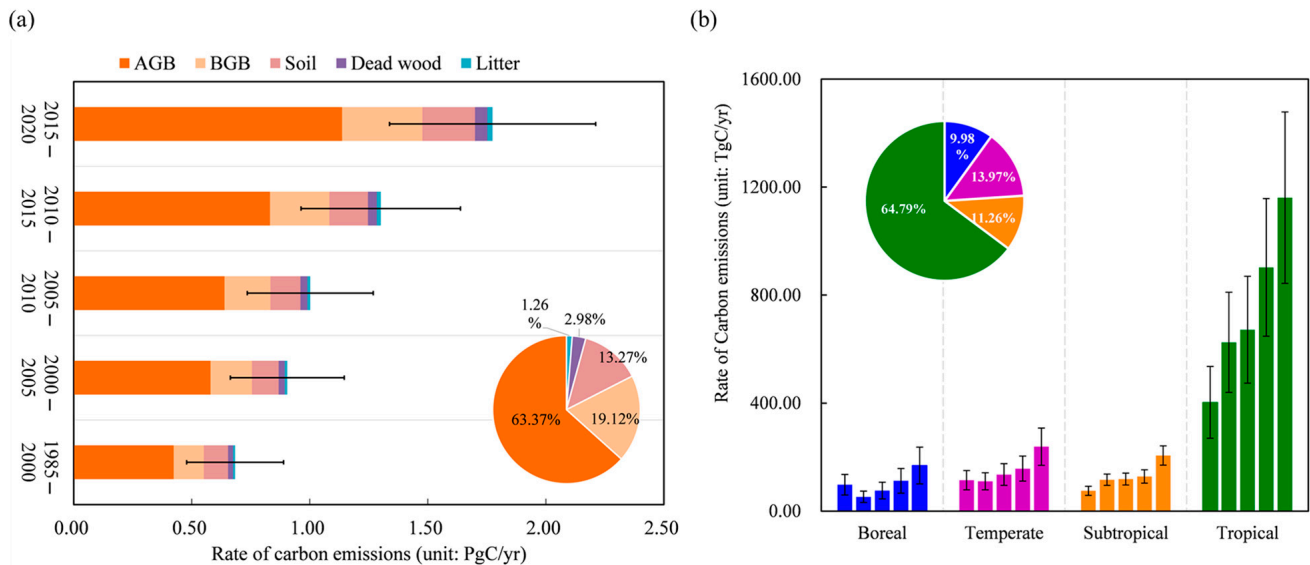


Figure 5. Changes in the spatial distribution of carbon emissions from forest loss in (a) the Amazon Basin; (b) Southeast Asia; and (c) the Congo Basin.

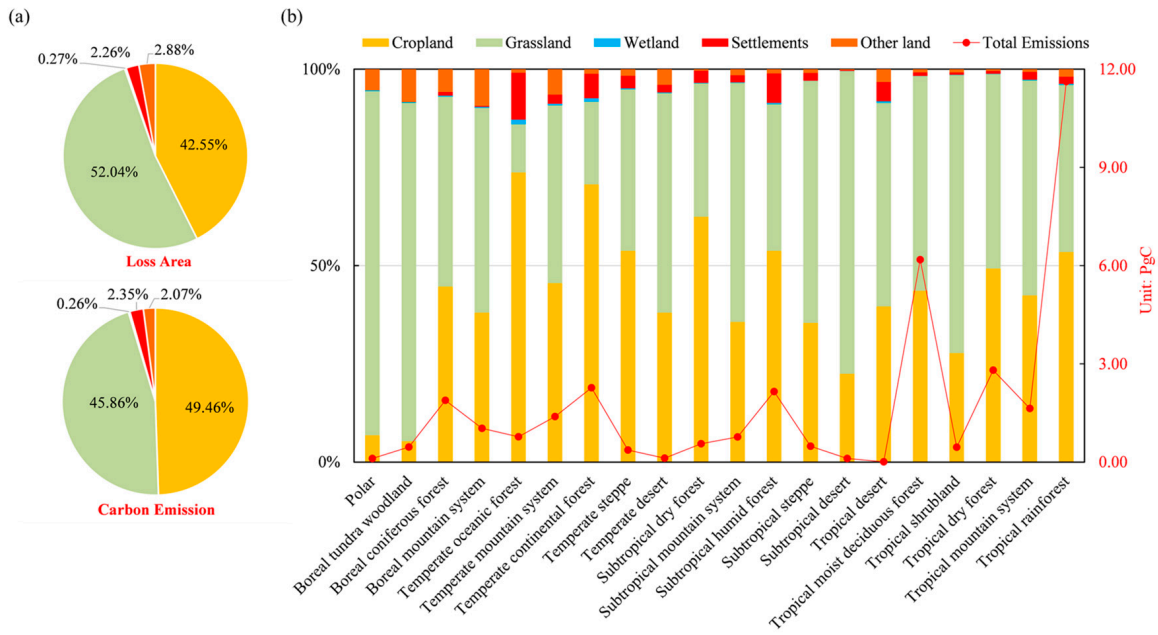


**Figure 6.** Rates of carbon emissions over time and global share in different (a) carbon pools and (b) climate zones.

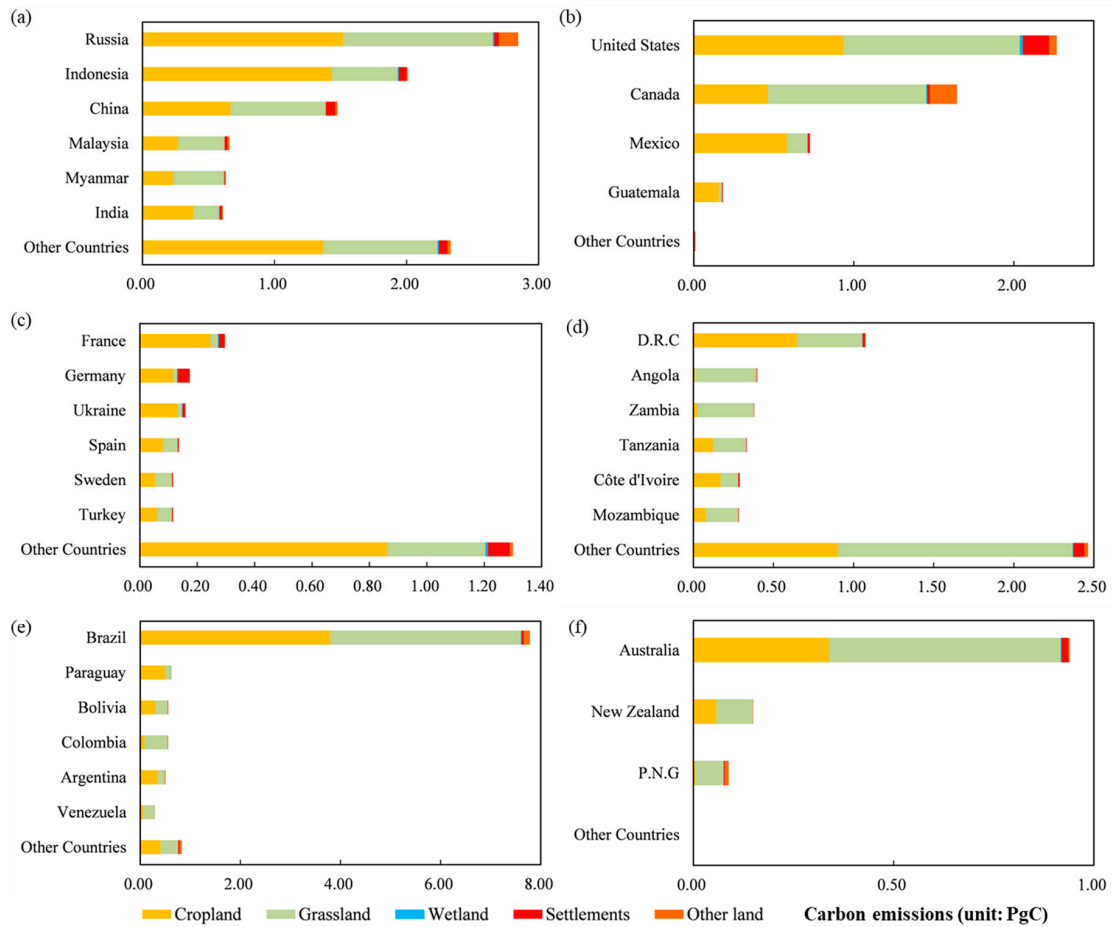
### 3.3. Contributions of Various Forest Conversion Types to Global Carbon Emissions

Figure 7 presents the amount and composition of carbon emissions within each ecological zone in terms of different forest conversion types. We can observe that grassland and cropland were the two most common land use types following forest loss, which dominated the global carbon emissions and accounted for about 45.86% and 49.46% of the total, respectively. Conversion of forest to the other types of land use occupied less than 5% (Figure 7a). The spatial distribution of carbon emissions from different conversion types was also clearly characterized. For example, the encroachment of cropland into forests typically occurred in ecological zones with a higher carbon intensity, such as tropical rainforest and subtropical humid forests. This results in it contributing a larger share of global carbon emissions compared to its share of the loss area (49.46% vs. 42.55%) (Figure 7a,b). In contrast, in mountainous and boreal zones, such as tropical mountain systems and boreal coniferous forests, carbon emissions caused by the replacement of forests by grassland usually dominated the overall emissions (Figure 7b).

We further compared the proportions of carbon emissions for conversion to cropland and grassland among countries. The results exhibited obvious regional characteristics. In most Asian countries, such as Indonesia and India, forests were more often encroached on by cropland than by grassland (Figure 8a); this was mainly due to the high land demand for arable use and for agroforestry crops arising from population growth and the development of plantation economies [62]. A similar situation also occurred in some European countries such as France and Ukraine (Figure 8c), which are important regions for grain exports. However, in Africa, the replacement of forests by grassland almost completely determined the carbon emissions from forest loss (Figure 8d). This was a result of a widely used method of acquiring arable land called “shift cultivation”, which usually involves burning forests and woodlands to create clear land for agricultural purposes [21]. In North America, the conversions of forests to cropland and grasslands were almost equally important in the United States, but cropland accounted for a higher share in Mexico and Guatemala (Figure 8b). A similar situation occurred in South America, where most countries, such as Paraguay and Argentina, experienced more cropland expansion into forest than grassland; while in Brazil, the two kinds of conversion contributed almost equally to carbon emissions (Figure 8e). It is also worth noting that in regions where forest wildfires are frequent, the replacement of forests by grassland usually dominated the carbon emissions; for example, in Australia and Canada, the emissions induced by conversion to grassland were more than twice as large as those produced by conversion to cropland (Figure 8b,f).



**Figure 7.** (a) Global share of five forest conversion types in forest loss area and carbon emissions; (b) the amount and composition of total carbon emissions in each ecological zone.



**Figure 8.** Total carbon emissions for different conversion types in major countries across six continents during 1985–2020: (a) Asia; (b) North America; (c) Europe; (d) Africa; (e) South America; (f) Oceania. Note: D.R.C and P.N.G are short for Democratic Republic of the Congo and Papua New Guinea, respectively.

### 3.4. Trends of Carbon Emissions in Mountainous Regions during 1985–2020

From 1985 to 2020, forest loss in mountainous regions worldwide resulted in total carbon emissions of approximately  $7.38 \pm 2.04$  PgC. This displayed a continuous accelerating trend, rising from  $155.60 \pm 45.54$  TgC/yr during 1985–2000 to  $362.49 \pm 94.11$  TgC/yr during 2015–2020. We further investigated the amounts of forest loss and resulting carbon emissions at different altitudes in mountainous regions during 1985–2020. Figure 9a shows that the forest loss at all altitudes in the mountainous regions experienced obvious increases, which was more serious at higher altitudes. Specifically, forest loss occurring at altitudes above 1000 m more than tripled. In some lower areas, such as altitudes below 200 m, forest loss also increased greatly, approximately doubling. For the resulting carbon emissions, regions at low altitudes dominated the global total throughout the study period (Figure 9a); and in the last five years, carbon emissions at high altitudes became more noticeable globally (Figure 9b).

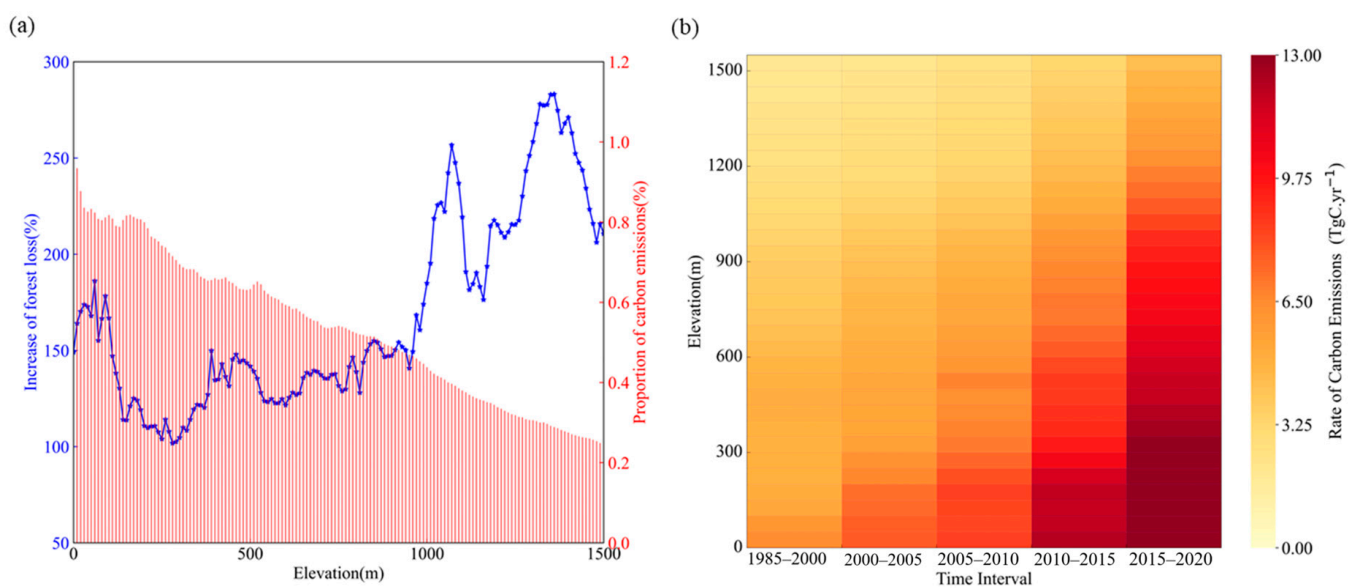


**Figure 9.** (a) The increase in mountainous forest loss area from 2015 to 2020 compared to that from 1985 to 2000 in different altitude intervals (blue line and left  $y$ -axis) and the global share of carbon emissions between 1985 and 2020 in different altitude intervals (red bar chart and right  $y$ -axis). (b) Rates of carbon emissions at different altitude intervals in mountainous regions.

## 4. Discussion

### 4.1. Comparisons with Previous Estimations

Many studies have focused on the global carbon emissions that are induced by forest loss, and their estimations vary widely due to differences in methodology, forest activity data, and carbon density parameters, among other factors [63]. The three Bookkeeping (BK) models adopted by the Global Carbon Project, namely, BLUE [64], H&N2017 [65], and OSCAR [66], all supply estimations of global carbon emissions from forest loss in the form of “legacy emissions,” which contain the contribution of carbon emissions due to historical forest loss. Conversely, the result herein was provided in the form of “committed emissions”, and it was lower compared to the average result of these three BK models ( $1.23 \pm 0.32$  PgC/yr vs.  $1.85 \pm 0.32$  PgC/yr) over the period of 2000–2020 (Table 2). Moreover, despite the increasing trend of forest loss during 2000–2020 that was observed by both Hansen et al. [27] and our study, the BK models’ results did not show either an increasing or even decreasing trend in the associated carbon emissions [5]. This is mainly due to the fact that the BK models rely on the land cover dataset derived from Food and Agriculture Organization statistics [15], which cannot accurately reflect the temporal dynamics of forest loss and lack spatially explicit information about forests in which a high carbon density

is found; meanwhile, this is not a problem for the GLC\_FCS30D dataset, which has high spatial and temporal resolutions.

**Table 2.** Carbon emissions from global forest loss under different methodologies (unit: PgC/yr).

Period	Previous Studies		This Study
2012–2021	Legacy	$1.8 \pm 0.4$ [67]	$1.54 \pm 0.39$
		1.96 [64]	
2000–2020	Legacy	1.41 [65]	$1.23 \pm 0.32$
		2.17 [66]	
	Committed	$2.21 \pm 0.68$ [28]	
		1.7 * [53]	$0.80 \pm 0.24$ *

\* These results only include carbon emissions from biomass pools.

We also compared our results with the most up-to-date national greenhouse gas inventory (NGHGI) database [68], which was established by integrating annual greenhouse gas inventories and a series of reports (e.g., national communications, biennial update reports, nationally determined contributions, etc.). Due to a lack of information on carbon emissions in several countries in this NGHGI database (e.g., China and India), the top-70 countries in terms of total carbon emissions during 2000–2020 were used for comparison, which accounted for about 93% of global emissions. The results showed good consistency between our estimates and the NGHGI database in most regions, including several dominating countries such as Brazil and Indonesia, with an overall  $R^2$  value of approximately 0.79 (Figure 10a). We further calculated the relative error in each country, which was defined as the absolute difference between our estimates and the NGHGI, divided by the NGHGI value. Figure 10b shows that the relative errors were mainly distributed around 0, especially for countries with high carbon emissions. There were also some countries whose relative error was much larger, particularly in countries with lower carbon emissions. This can be attributed to the accuracy of the products that were used in this study and the NGHGI database.

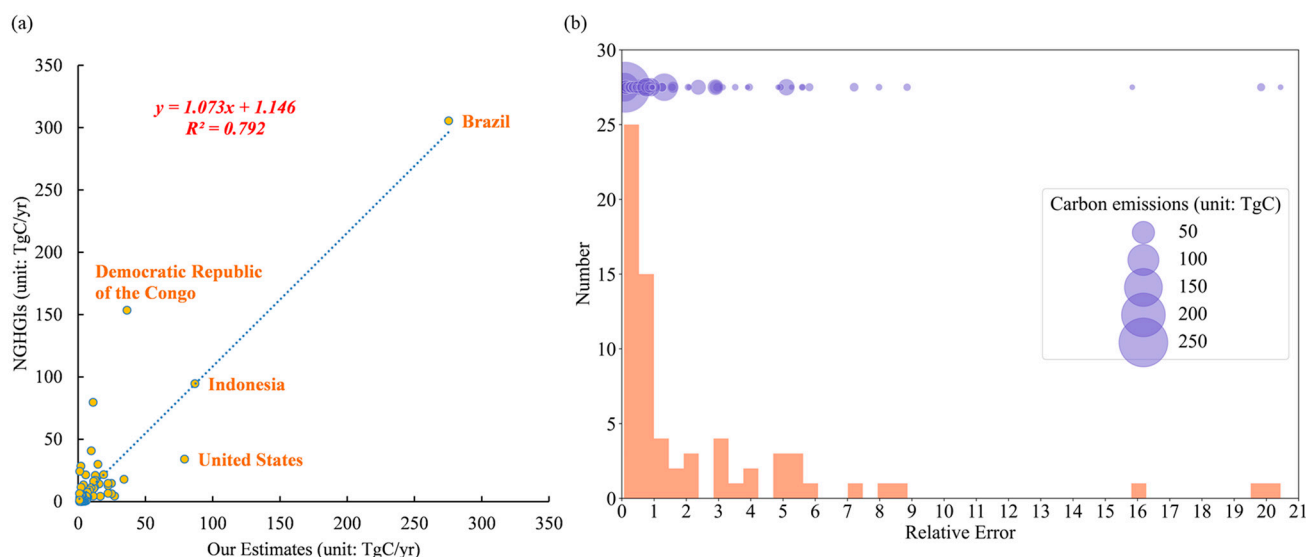


**Figure 10.** Comparison of results for major countries in terms of total emissions: (a) the scatterplot of our estimates against the NGHGI database; (b) the histogram of relative errors (ratio of the absolute difference between our estimates and NGHGI relative to NGHGI). Note: the purple bubbles represent the carbon emissions of each country whose relative error fell into each bin of the histogram.

Some researchers have also applied remote sensing-based methods to estimate the committed carbon emissions from forest loss. For example, Xu et al. [53] suggested that global forest loss contributed a biomass carbon loss of 1.7 Pg per year during 2000–2019,

which was mainly assessed by overlaying the annual global AGB maps at 10 km grid cells and the GFCC products. Harris et al. [28] also estimated the global greenhouse gas emissions induced by forest loss by combining GFCC maps, a global AGB product, and parameters such as carbon removal factors from the IPCC Guidelines. However, both of their conclusions are higher than ours (Table 2).

These discrepancies can be attributed to two reasons. First, the overestimation of forest loss area has always existed in the GFCC dataset [69]. For example, oil palm plantations in Malaysia and Indonesia have undergone substantial establishment and abandonment, and even the net increase was up to about 13.46 Mha during 2000–2016 [70]; such agricultural rotation activities are identified as forest loss in the GFCC dataset. Conversely, the GLC\_FCS30D dataset, which has a fine classification system, successfully distinguishes these agricultural tree crops from forests [29]. Second, different carbon stock datasets were applied in the estimation process. The 10 km gridded biomass products used by Xu et al. [53] were too coarse to capture the spatial details of AGB compared to the fine-spatial-resolution datasets that were used in our study, especially in heterogeneous regions. Harris et al. [28] directly used the carbon removal factors recommended by the IPCC to characterize the dynamics of biomass carbon pools, which introduced considerable uncertainty into the final estimations. Furthermore, considering the limited accuracy at the pixel scale for these existing coarse biomass products, direct overlaying of the biomass data and forest loss maps can yield inaccurate results [71]. Therefore, we chose to establish the LUT of carbon density for different forest types at each 0.1° grid by co-locating high-spatial-resolution biomass data with land cover maps.

#### 4.2. Limitations and Uncertainties

In this study, we focused on the carbon emissions induced by global forest loss, while there are also various carbon emissions from fire, agriculture, shipping, etc. For example, carbon emissions due to fire ranged from 1.6 to 1.7 PgC/yr over the period of 2013–2022 [5]; international aviation and shipping collectively accounted for 17.16 TgC/yr in global carbon emissions during 1985–2020 [72]; and shift cultivation—an agricultural activity that is prevalent in the tropical regions—led to 0.8 PgC/yr of carbon emissions over the period of 2013–2022 [5]. These sources are closely linked to forest loss, which is evident in phenomena like the frequent encroachment of agricultural expansion into forests [62] and the accelerating forest wildfires [73]. Therefore, it is worthwhile to clarify their relationships and combined impacts on carbon emissions in our future studies.

Concerning the uncertainties in our study, we derived the global forest conversion area through overlaying land cover maps across multiple periods and constructing the land cover transfer matrices [2,10,11,60,74]. This practice is susceptible to classification errors in land cover maps from different periods, which can lead to inaccurate estimation of the forest conversion area. However, quantifying the uncertainty of forest conversion areas derived from a land cover dataset and obtaining an unbiased estimation is always difficult and challenging, especially on a global scale and at fine spatial resolutions such as 30 m. For example, Olofsson et al. [75] proposed a method that combines land cover maps and validation samples to provide an unbiased estimation of the land cover change area, while there is currently a lack of publicly available global validation datasets at such a high spatial resolution. Thus, in the future, it will be worth designing and constructing a set of validation samples for testing the accuracy of the forest cover change [76], so as to achieve an unbiased estimation of the global forest conversion area and reduce its impact on the uncertainty of carbon emissions.

Furthermore, constrained by the current lack of time series data on SOC at the global scale, and the absence of an uncertainty layer in the SOC data used for this research, we did not incorporate the uncertainty of SOC emissions in the final results. Meanwhile, considering that SOC emissions constitute less than 14% of the total carbon emissions, this omission has little impact on our conclusions. In addition, given that the annual changes in the global forest carbon stocks are negligible relative to their total [53], we ignored the temporal

variation in forest biomass in each 0.1° grid due to its limited interference with the final results. And with the development of new high-spatial-resolution satellite missions such as BIOMASS, numerous repeated measurements will enhance our understanding of the temporal trends in forest biomass and significantly contribute to reducing their uncertainty.

#### 4.3. Implications for Slowing Global Carbon Emissions from Forest Loss

The results of this study show that carbon emissions in tropical zones have not declined as expected, and they still dominate the global carbon emissions from forest loss due to increasing forest loss and a high carbon density. Past efforts to reduce forest loss in tropical zones have not been maintained, and there is still a need for sustained attention and regular monitoring and assessment in the future. Moreover, in mountainous regions, where ecosystems are often more fragile than in the plains, our results indicate that the carbon emissions from forest loss have also experienced a doubling acceleration, and the emissions at high altitudes have become more obvious than before. Considering forests' important role in mountainous ecosystems, large forest loss will result in the destruction of ecosystem barriers and cause habitat fragmentation for many plants and animals, posing a threat to biodiversity. It will also cause soil erosion, alter the local climate, and finally, increase the likelihood of forest biomass being destroyed [77]. Therefore, forest conservation measures should be urgently implemented throughout all mountainous regions, especially at high altitudes.

## 5. Conclusions

This study quantified the global carbon emissions from forest loss during 1985–2020 based on the method that is recommended by the IPCC Guidelines. This was achieved by improving the estimation of the forest loss area based on a novel fine-resolution global land cover product and enhancing the information about the densities of different carbon pools using multi-sourced carbon stock maps. Over these 35 years, we observed a continuous acceleration of global forest loss, about 582.17 Mha in total, which led to total committed carbon emissions of about  $35.22 \pm 9.38$  PgC. The tropical zones dominated the global carbon emissions (~2/3) due to their higher carbon density and greater forest loss. Moreover, global emissions have also experienced a doubling growth, rising from  $0.69 \pm 0.21$  PgC/yr in 1985–2000 to  $1.77 \pm 0.44$  PgC/yr in 2015–2020. As the top-two land use types following forest loss, grassland and cropland accounted for about 45.86% and 49.46% of the total emissions, respectively, and cropland usually invaded forests of higher carbon densities. Furthermore, the loss of mountainous forest has also increased rapidly, particularly in areas above 1000 m in altitude, where forest loss has more than tripled, and the resulting carbon emissions are more pronounced than before. This new estimation of global carbon emissions suggests that more efforts are needed to reduce forest loss, especially in tropical rainforests and mountainous regions.

**Author Contributions:** Conceptualization, L.L., W.L. and X.Z.; funding acquisition, L.L. and X.Z.; methodology, L.L., W.L. and X.Z.; software, W.L.; formal analysis, L.L. and W.L.; writing—original draft preparation, W.L.; writing—review and editing, L.L., X.Z., H.X., T.Z., J.W. and Z.L. All authors have read and agreed to the published version of the manuscript.

**Funding:** This research was funded by the National Natural Science Foundation of China (Grant No. 41825002, Grant No. 42201499) and the Open Research Program of the International Research Center of Big Data for Sustainable Development Goals (Grant No. CBAS2022ORP03).

**Data Availability Statement:** The land cover dataset GLC\_FCS30D is available at <https://zenodo.org/record/8239305> (accessed on 12 August 2023). The five multiple biomass datasets are available at <https://data.globalforestwatch.org/> (accessed on 14 June 2023), <https://data.ess-dive.lbl.gov/> (accessed on 5 November 2023), <http://www.glass.umd.edu/index.html> (accessed on 3 December 2023), <https://doi.org/10.1594/PANGAEA.894711> (accessed on 3 December 2023), and <https://daac.ornl.gov/> (accessed on 27 December 2023) in the order described in the text. The SOC dataset is available at <https://zenodo.org/record/5040380> (accessed on 27 October 2023). The ASTER GDEM V3 dataset

is available at <https://earthdata.nasa.gov/> (accessed on 14 June 2023). The GMBA dataset is available at [https://ilias.unibe.ch/goto\\_ilias3\\_unibe\\_cat\\_1000515.html](https://ilias.unibe.ch/goto_ilias3_unibe_cat_1000515.html) (accessed on 15 June 2023). The Administrative boundary data are available at <https://gadm.org/> (accessed on 27 August 2023). The global forest ecological zone map is available at <https://data.apps.fao.org/map/catalog/srv/eng/catalog.search#/home> (accessed on 27 October 2023).

**Acknowledgments:** The authors sincerely thank the organizations and individuals who generously provided the free datasets used in this research.

**Conflicts of Interest:** The authors declare no conflicts of interest.

## Appendix A

**Table A1.** Relationship between land cover types in the GLC\_FCS30D and IPCC categories and the percentage of SOC emissions for different conversion types.

Fine-Resolution Classification System	Land Cover Code	IPCC Category	Percentage of SOC Emissions
Rainfed cropland	10	Cropland	20%
Herbaceous cover	11		
Tree or shrub cover (Orchard)	12		
Irrigated cropland	20		
Open evergreen broad-leaved forest	51	Forest land	0%
Closed evergreen broad-leaved forest	52		
Open deciduous broad-leaved forest (0.15 < fc < 0.4)	61		
Closed deciduous broad-leaved forest (fc > 0.4)	62		
Open evergreen needle-leaved forest (0.15 < fc < 0.4)	71		
Closed evergreen needle-leaved forest (fc > 0.4)	72		
Open deciduous needle-leaved forest (0.15 < fc < 0.4)	81		
Closed deciduous needle-leaved forest (fc > 0.4)	82		
Open mixed leaf forest (broad-leaved and needle-leaved)	91		
Closed mixed leaf forest (broad-leaved and needle-leaved)	92		
Shrubland	120	Grassland	11%
Evergreen shrubland	121		
Deciduous shrubland	122		
Grassland	130		
Lichens and mosses	140		
Sparse vegetation (fc < 0.15)	150		
Sparse shrubland (fc < 0.15)	152		
Sparse herbaceous (fc < 0.15)	153		
Swamp	181	Wetlands	5%
Marsh	182		
Flooded flat	183		
Saline	184		
Mangrove	185		
Salt marsh	186		
Tidal flat	187		
Impervious surfaces	190	Settlements	20%
Bare areas	200	Other land	5%
Consolidated bare areas	201		
Unconsolidated bare areas	202		
Permanent ice and snow	220		
Water body	210		

**Table A2.** The 21 FAO ecological zones and their climate types and the relationships between dead wood and litter carbon stock and AGB carbon stock in each ecological zone.

Code	Name	Climate Zone	Ratio of Dead Wood to AGB	Ratio of Litter to AGB
1	Polar		8%	4%
2	Boreal tundra woodland		8%	4%
3	Boreal coniferous forest	Boreal	8%	4%
4	Boreal mountain system		8%	4%
5	Water		-	-
6	Temperate oceanic forest		8%	4%
7	Temperate mountain system		8%	4%
8	Temperate continental forest	Temperate	8%	4%
9	Temperate steppe		8%	4%
10	Temperate desert		8%	4%
11	Subtropical dry forest		2%	4%
12	Subtropical mountain system		7%	1%
13	Subtropical humid forest	Subtropical	1%	1%
14	Subtropical steppe		2%	4%
15	Subtropical desert		2%	4%
16	Tropical desert		2%	4%
17	Tropical moist deciduous forest		1%	1%
18	Tropical shrubland	Tropical	2%	4%
19	Tropical dry forest		2%	4%
20	Tropical mountain system		7%	1%
21	Tropical rainforest		6%	1%

## References

1. FAO. *Global Forest Resources Assessment 2020: Main Report*; Food and Agriculture Organization of the United Nations: Rome, Italy, 2020. [\[CrossRef\]](#)
2. Winkler, K.; Fuchs, R.; Rounsevell, M.; Herold, M. Global land use changes are four times greater than previously estimated. *Nat. Commun.* **2021**, *12*, 2501. [\[CrossRef\]](#) [\[PubMed\]](#)
3. Avissar, R.; Werth, D. Global Hydroclimatological Teleconnections Resulting from Tropical Deforestation. *J. Hydrometeorol.* **2005**, *6*, 134–145. [\[CrossRef\]](#)
4. Harris, N.L.; Brown, S.; Hagen, S.C.; Saatchi, S.S.; Petrova, S.; Salas, W.; Hansen, M.C.; Potapov, P.V.; Lotsch, A. Baseline map of carbon emissions from deforestation in tropical regions. *Science* **2012**, *336*, 1573–1576. [\[CrossRef\]](#) [\[PubMed\]](#)
5. Friedlingstein, P.; O’Sullivan, M.; Jones, M.W.; Andrew, R.M.; Bakker, D.C.E.; Hauck, J.; Landschützer, P.; Le Quéré, C.; Luijckx, I.T.; Peters, G.P.; et al. Global Carbon Budget 2023. *Earth Syst. Sci. Data* **2023**, *15*, 5301–5369. [\[CrossRef\]](#)
6. Houghton, R.A. Revised estimates of the annual net flux of carbon to the atmosphere from changes in land use and land management 1850–2000. *Tellus B Chem. Phys. Meteorol.* **2003**, *55*, 378–390.
7. Bullock, E.L.; Woodcock, C.E. Carbon loss and removal due to forest disturbance and regeneration in the Amazon. *Sci. Total Environ.* **2021**, *764*, 142839. [\[CrossRef\]](#)
8. Tang, X.; Woodcock, C.E.; Olofsson, P.; Hutyrá, L.R. Spatiotemporal assessment of land use/land cover change and associated carbon emissions and uptake in the Mekong River Basin. *Remote Sens. Environ.* **2021**, *256*, 112336. [\[CrossRef\]](#)
9. Houghton, R.A.; House, J.I.; Pongratz, J.; Van Der Werf, G.R.; Defries, R.S.; Hansen, M.C.; Le Quéré, C.; Ramankutty, N. Carbon emissions from land use and land-cover change. *Biogeosciences* **2012**, *9*, 5125–5142. [\[CrossRef\]](#)
10. Lai, L.; Huang, X.; Yang, H.; Chuai, X.; Zhang, M.; Zhong, T.; Chen, Z.; Chen, Y.; Wang, X.; Thompson, J.R. Carbon emissions from land-use change and management in China between 1990 and 2010. *Sci. Adv.* **2016**, *2*, e1601063. [\[CrossRef\]](#)
11. Zhu, E.; Deng, J.; Zhou, M.; Gan, M.; Jiang, R.; Wang, K.; Shahtahmassebi, A. Carbon emissions induced by land-use and land-cover change from 1970 to 2010 in Zhejiang, China. *Sci. Total Environ.* **2019**, *646*, 930–939. [\[CrossRef\]](#)
12. Baccini, A.; Walker, W.; Carvalho, L.; Farina, M.; Sulla-Menashe, D.; Houghton, R. Tropical forests are a net carbon source based on aboveground measurements of gain and loss. *Science* **2017**, *358*, 230–234. [\[CrossRef\]](#)
13. Ciais, P.; Bastos, A.; Chevallier, F.; Lauerwald, R.; Poulter, B.; Canadell, J.G.; Hugelius, G.; Jackson, R.B.; Jain, A.; Jones, M. Definitions and methods to estimate regional land carbon fluxes for the second phase of the REgional Carbon Cycle Assessment and Processes Project (RECCAP-2). *Geosci. Model Dev.* **2022**, *15*, 1289–1316. [\[CrossRef\]](#)
14. Klein Goldewijk, K.; Beusen, A.; de Vos, M.; van Dreht, G. The HYDE 3.1 spatially explicit database of human induced land use change over the past 12,000 years. *Glob. Ecol. Biogeogr.* **2011**, *20*, 73–86. [\[CrossRef\]](#)
15. Hurtt, G.C.; Chini, L.; Sahajpal, R.; Frothingham, S.; Bodirsky, B.L.; Calvin, K.; Doelman, J.C.; Fisk, J.; Fujimori, S.; Klein Goldewijk, K. Harmonization of global land use change and management for the period 850–2100 (LUH2) for CMIP6. *Geosci. Model Dev.* **2020**, *13*, 5425–5464. [\[CrossRef\]](#)

16. FAOSTAT. FAOSTAT: Food and Agriculture Organization Statistics Division. Available online: <http://faostat.fao.org/> (accessed on 25 September 2023).
17. Bastos, A.; Ciais, P.; Sitch, S.; Aragão, L.E.; Chevallier, F.; Fawcett, D.; Rosan, T.M.; Saunois, M.; Günther, D.; Perugini, L. On the use of Earth Observation to support estimates of national greenhouse gas emissions and sinks for the Global stocktake process: Lessons learned from ESA-CCI RECCAP2. *Carbon Balance Manag.* **2022**, *17*, 15. [[CrossRef](#)] [[PubMed](#)]
18. Brinck, K.; Fischer, R.; Groeneveld, J.; Lehmann, S.; Dantas De Paula, M.; Pütz, S.; Sexton, J.O.; Song, D.; Huth, A. High resolution analysis of tropical forest fragmentation and its impact on the global carbon cycle. *Nat. Commun.* **2017**, *8*, 14855. [[CrossRef](#)] [[PubMed](#)]
19. Hansen, M.C.; Wang, L.; Song, X.-P.; Tyukavina, A.; Turubanova, S.; Potapov, P.V.; Stehman, S.V. The fate of tropical forest fragments. *Sci. Adv.* **2020**, *6*, eaax8574. [[CrossRef](#)] [[PubMed](#)]
20. Reiner, F.; Brandt, M.; Tong, X.; Skole, D.; Kariryaa, A.; Ciais, P.; Davies, A.; Hiernaux, P.; Chave, J.; Mugabowindekwe, M. More than one quarter of Africa's tree cover is found outside areas previously classified as forest. *Nat. Commun.* **2023**, *14*, 2258. [[CrossRef](#)] [[PubMed](#)]
21. Curtis, P.G.; Slay, C.M.; Harris, N.L.; Tyukavina, A.; Hansen, M.C. Classifying drivers of global forest loss. *Science* **2018**, *361*, 1108–1111. [[CrossRef](#)] [[PubMed](#)]
22. Riva, F.; Martin, C.J.; Millard, K.; Fahrig, L. Loss of the world's smallest forests. *Glob. Chang. Biol.* **2022**, *28*, 7164–7166. [[CrossRef](#)] [[PubMed](#)]
23. Gong, P.; Wang, J.; Yu, L.; Zhao, Y.; Zhao, Y.; Liang, L.; Niu, Z.; Huang, X.; Fu, H.; Liu, S. Finer resolution observation and monitoring of global land cover: First mapping results with Landsat TM and ETM+ data. *Int. J. Remote Sens.* **2013**, *34*, 2607–2654. [[CrossRef](#)]
24. Chen, J.; Chen, J.; Liao, A.; Cao, X.; Chen, L.; Chen, X.; He, C.; Han, G.; Peng, S.; Lu, M. Global land cover mapping at 30 m resolution: A POK-based operational approach. *ISPRS J. Photogramm. Remote Sens.* **2015**, *103*, 7–27. [[CrossRef](#)]
25. Mi, J.; Liu, L.; Zhang, X.; Chen, X.; Gao, Y.; Xie, S. Impact of geometric misregistration in GlobeLand30 on land-cover change analysis, a case study in China. *J. Appl. Remote Sens.* **2022**, *16*, 014516. [[CrossRef](#)]
26. Friedl, M.A.; Woodcock, C.E.; Olofsson, P.; Zhu, Z.; Loveland, T.; Stanimirova, R.; Arevalo, P.; Bullock, E.; Hu, K.-T.; Zhang, Y. Medium spatial resolution mapping of global land cover and land cover change across multiple decades from landsat. *Front. Remote Sens.* **2022**, *3*, 894571. [[CrossRef](#)]
27. Hansen, M.C.; Potapov, P.V.; Moore, R.; Hancher, M.; Turubanova, S.A.; Tyukavina, A.; Thau, D.; Stehman, S.V.; Goetz, S.J.; Loveland, T.R.; et al. High-Resolution Global Maps of 21st-Century Forest Cover Change. *Science* **2013**, *342*, 850–853. [[CrossRef](#)] [[PubMed](#)]
28. Harris, N.L.; Gibbs, D.A.; Baccini, A.; Birdsey, R.A.; de Bruin, S.; Farina, M.; Fatoyinbo, L.; Hansen, M.C.; Herold, M.; Houghton, R.A.; et al. Global maps of twenty-first century forest carbon fluxes. *Nat. Clim. Chang.* **2021**, *11*, 234–240. [[CrossRef](#)]
29. Zhang, X.; Zhao, T.; Xu, H.; Liu, W.; Wang, J.; Chen, X.; Liu, L. GLC\_FCS30D: The first global 30-m land-cover dynamic monitoring product with a fine classification system from 1985 to 2022 using dense time-series Landsat imagery and continuous change-detection method. *Earth Syst. Sci. Data Discuss.* **2023**, *2023*, 1–32.
30. Liu, L. *GLC\_FCS30D: Global 30-m Land-Cover Dynamic Monitoring Product with a Fine Classification System from 1985 to 2022*; International Research Center of Big Data for Sustainable Development Goals: Beijing, China, 2023. [[CrossRef](#)]
31. IPCC. *2006 IPCC Guidelines for National Greenhouse Gas Inventories, Prepared by the National Greenhouse Gas Inventories Programme*; Eggleston, H.S., Buendia, L., Miwa, K., Ngara, T., Tanabe, K., Eds.; IGES: Hayama, Japan, 2006.
32. UNFCCC. Methodological Tool: Estimation of Carbon Stocks and Change in Carbon Stocks in Dead Wood and Litter in A/R CDM Project Activities. 2020. Available online: <https://cdm.unfccc.int/methodologies/ARmethodologies/tools/ar-amtool-12-v3.0.pdf> (accessed on 27 June 2023).
33. Duncanson, L.; Kellner, J.R.; Armston, J.; Dubayah, R.; Minor, D.M.; Hancock, S.; Healey, S.P.; Patterson, P.L.; Saarela, S.; Marselis, S. Aboveground biomass density models for NASA's Global Ecosystem Dynamics Investigation (GEDI) lidar mission. *Remote Sens. Environ.* **2022**, *270*, 112845. [[CrossRef](#)]
34. Gibbs, H.K.; Ruesch, A. *New IPCC Tier-1 Global Biomass Carbon Map for the Year 2000*; CDIAC, ESS-DIVE Repository: USA, 2008. [[CrossRef](#)]
35. Santoro, M.; Cartus, O.; Carvalhais, N.; Rozendaal, D.M.A.; Avitabile, V.; Araza, A.; de Bruin, S.; Herold, M.; Quegan, S.; Rodríguez-Veiga, P.; et al. The global forest above-ground biomass pool for 2010 estimated from high-resolution satellite observations. *Earth Syst. Sci. Data* **2021**, *13*, 3927–3950. [[CrossRef](#)]
36. Avitabile, V.; Herold, M.; Heuvelink, G.B.; Lewis, S.L.; Phillips, O.L.; Asner, G.P.; Armston, J.; Ashton, P.S.; Banin, L.; Bayol, N. An integrated pan-tropical biomass map using multiple reference datasets. *Glob. Chang. Biol.* **2016**, *22*, 1406–1420. [[CrossRef](#)]
37. Spawn, S.A.; Sullivan, C.C.; Lark, T.J.; Gibbs, H.K. Harmonized global maps of above and belowground biomass carbon density in the year 2010. *Sci. Data* **2020**, *7*, 112. [[CrossRef](#)]
38. Zhang, Y.; Liang, S. Fusion of multiple gridded biomass datasets for generating a global forest aboveground biomass map. *Remote Sens.* **2020**, *12*, 2559. [[CrossRef](#)]
39. Veldkamp, E.; Schmidt, M.; Powers, J.S.; Corre, M.D. Deforestation and reforestation impacts on soils in the tropics. *Nat. Rev. Earth Environ.* **2020**, *1*, 590–605. [[CrossRef](#)]

40. Nachtergaele, F.; Velthuizen, H.; Verelst, L.; Wiberg, D. *Harmonized World Soil Database (Hwsd)*; Food and Agriculture Organization of the United Nations: Rome, Italy, 2009.
41. Hengl, T.; Mendes de Jesus, J.; Heuvelink, G.B.; Ruiperez Gonzalez, M.; Kilibarda, M.; Blagotić, A.; Shangguan, W.; Wright, M.N.; Geng, X.; Bauer-Marschallinger, B. SoilGrids250m: Global gridded soil information based on machine learning. *PLoS ONE* **2017**, *12*, e0169748. [[CrossRef](#)]
42. Xie, E.; Zhang, X.; Lu, F.; Peng, Y.; Chen, J.; Zhao, Y. Integration of a process-based model into the digital soil mapping improves the space-time soil organic carbon modelling in intensively human-impacted area. *Geoderma* **2022**, *409*, 115599. [[CrossRef](#)]
43. Zhang, X.; Liu, L.; Chen, X.; Gao, Y.; Xie, S.; Mi, J. GLC\_FCS30: Global land-cover product with fine classification system at 30 m using time-series Landsat imagery. *Earth Syst. Sci. Data* **2021**, *13*, 2753–2776. [[CrossRef](#)]
44. Zhang, X.; Liu, L.; Zhao, T.; Chen, X.; Lin, S.; Wang, J.; Mi, J.; Liu, W. GWL\_FCS30: A global 30 m wetland map with a fine classification system using multi-sourced and time-series remote sensing imagery in 2020. *Earth Syst. Sci. Data* **2023**, *15*, 265–293. [[CrossRef](#)]
45. Zhang, X.; Liu, L.; Zhao, T.; Gao, Y.; Chen, X.; Mi, J. GISD30: Global 30 m impervious-surface dynamic dataset from 1985 to 2020 using time-series Landsat imagery on the Google Earth Engine platform. *Earth Syst. Sci. Data* **2022**, *14*, 1831–1856. [[CrossRef](#)]
46. Roy, D.P.; Wulder, M.A.; Loveland, T.R.; Woodcock, C.E.; Allen, R.G.; Anderson, M.C.; Helder, D.; Irons, J.R.; Johnson, D.M.; Kennedy, R. Landsat-8: Science and product vision for terrestrial global change research. *Remote Sens. Environ.* **2014**, *145*, 154–172. [[CrossRef](#)]
47. Yang, L.; Liang, S.; Zhang, Y. A new method for generating a global forest aboveground biomass map from multiple high-level satellite products and ancillary information. *IEEE Journal of Selected Topics in Applied Earth Observations and Remote Sensing* **2020**, *13*, 2587–2597. [[CrossRef](#)]
48. Dubayah, R.; Armston, J.; Healey, S.; Yang, Z.; Patterson, P.; Saarela, S.; Stahl, G.; Duncanson, L.; Kellner, J. *GEDI L4B Gridded Aboveground Biomass Density*; Version 2; ORNL DAAC: Oak Ridge, TN, USA, 2022. [[CrossRef](#)]
49. Fujisada, H.; Bailey, G.B.; Kelly, G.G.; Hara, S.; Abrams, M.J. Aster dem performance. *IEEE Trans. Geosci. Remote Sens.* **2005**, *43*, 2707–2714. [[CrossRef](#)]
50. Fujisada, H.; Urai, M.; Iwasaki, A. Advanced methodology for ASTER DEM generation. *IEEE Trans. Geosci. Remote Sens.* **2011**, *49*, 5080–5091. [[CrossRef](#)]
51. Körner, C.; Jetz, W.; Paulsen, J.; Payne, D.; Rudmann-Maurer, K.; Spehn, E.M. A global inventory of mountains for bio-geographical applications. *Alp. Bot.* **2017**, *127*, 1–15. [[CrossRef](#)]
52. FAO. *Global Ecological Zones for FAO Forest Reporting: 2010 Update*; Forest Resources Assessment Working Paper N; FAO: Rome, Italy, 2012.
53. Xu, L.; Saatchi, S.S.; Yang, Y.; Yu, Y.; Pongratz, J.; Bloom, A.A.; Bowman, K.; Worden, J.; Liu, J.; Yin, Y. Changes in global terrestrial live biomass over the 21st century. *Sci. Adv.* **2021**, *7*, eabe9829. [[CrossRef](#)]
54. Zarin, D.J.; Harris, N.L.; Baccini, A.; Aksenov, D.; Hansen, M.C.; Azevedo-Ramos, C.; Azevedo, T.; Margono, B.A.; Alencar, A.C.; Gabris, C. Can carbon emissions from tropical deforestation drop by 50% in 5 years? *Glob. Chang. Biol.* **2016**, *22*, 1336–1347. [[CrossRef](#)]
55. Feng, Y.; Zeng, Z.; Searchinger, T.D.; Ziegler, A.D.; Wu, J.; Wang, D.; He, X.; Elsen, P.R.; Ciais, P.; Xu, R.; et al. Doubling of annual forest carbon loss over the tropics during the early twenty-first century. *Nat. Sustain.* **2022**, *5*, 444–451. [[CrossRef](#)]
56. Davis, S.J.; Burney, J.A.; Pongratz, J.; Caldeira, K. Methods for attributing land-use emissions to products. *Carbon Manag.* **2014**, *5*, 233–245. [[CrossRef](#)]
57. Guo, L.B.; Gifford, R.M. Soil carbon stocks and land use change: A meta analysis. *Glob. Chang. Biol.* **2002**, *8*, 345–360. [[CrossRef](#)]
58. Don, A.; Schumacher, J.; Freibauer, A. Impact of tropical land-use change on soil organic carbon stocks—a meta-analysis. *Glob. Chang. Biol.* **2011**, *17*, 1658–1670. [[CrossRef](#)]
59. Zeng, Z.; Estes, L.; Ziegler, A.D.; Chen, A.; Searchinger, T.; Hua, F.; Guan, K.; Jintrawet, A.; Wood, E.F. Highland cropland expansion and forest loss in Southeast Asia in the twenty-first century. *Nat. Geosci.* **2018**, *11*, 556–562. [[CrossRef](#)]
60. Yang, C.; Liu, H.; Li, Q.; Wang, X.; Ma, W.; Liu, C.; Fang, X.; Tang, Y.; Shi, T.; Wang, Q. Human expansion into Asian highlands in the 21st Century and its effects. *Nat. Commun.* **2022**, *13*, 4955. [[CrossRef](#)]
61. Abrams, M.; Crippen, R.; Fujisada, H. ASTER global digital elevation model (GDEM) and ASTER global water body dataset (ASTWBD). *Remote Sens.* **2020**, *12*, 1156. [[CrossRef](#)]
62. Xu, Y.; Yu, L.; Ciais, P.; Li, W.; Santoro, M.; Yang, H.; Gong, P. Recent expansion of oil palm plantations into carbon-rich forests. *Nat. Sustain.* **2022**, *5*, 574–577. [[CrossRef](#)]
63. Grassi, G.; House, J.; Kurz, W.A.; Cescatti, A.; Houghton, R.A.; Peters, G.P.; Sanz, M.J.; Viñas, R.A.; Alkama, R.; Arneeth, A. Reconciling global-model estimates and country reporting of anthropogenic forest CO<sub>2</sub> sinks. *Nat. Clim. Chang.* **2018**, *8*, 914–920. [[CrossRef](#)]
64. Hansis, E.; Davis, S.J.; Pongratz, J. Relevance of methodological choices for accounting of land use change carbon fluxes. *Glob. Biogeochem. Cycles* **2015**, *29*, 1230–1246. [[CrossRef](#)]
65. Houghton, R.A.; Nassikas, A.A. Global and regional fluxes of carbon from land use and land cover change 1850–2015. *Glob. Biogeochem. Cycles* **2017**, *31*, 456–472. [[CrossRef](#)]
66. Gasser, T.; Crepin, L.; Quilcaille, Y.; Houghton, R.A.; Ciais, P.; Obersteiner, M. Historical CO<sub>2</sub> emissions from land use and land cover change and their uncertainty. *Biogeosciences* **2020**, *17*, 4075–4101. [[CrossRef](#)]

67. Friedlingstein, P.; O'Sullivan, M.; Jones, M.W.; Andrew, R.M.; Gregor, L.; Hauck, J.; Le Quéré, C.; Luijkx, I.T.; Olsen, A.; Peters, G.P.; et al. Global Carbon Budget 2022. *Earth Syst. Sci. Data* **2022**, *14*, 4811–4900. [[CrossRef](#)]
68. Grassi, G.; Schwingshackl, C.; Gasser, T.; Houghton, R.A.; Sitch, S.; Canadell, J.G.; Cescatti, A.; Ciais, P.; Federici, S.; Friedlingstein, P. Harmonising the land-use flux estimates of global models and national inventories for 2000–2020. *Earth Syst. Sci. Data* **2023**, *15*, 1093–1114. [[CrossRef](#)]
69. Tropek, R.; Sedláček, O.; Beck, J.; Keil, P.; Musilová, Z.; Šímová, I.; Storch, D. Comment on “High-resolution global maps of 21st-century forest cover change”. *Science* **2014**, *344*, 981. [[CrossRef](#)]
70. Xu, Y.; Yu, L.; Li, W.; Ciais, P.; Cheng, Y.; Gong, P. Annual oil palm plantation maps in Malaysia and Indonesia from 2001 to 2016. *Earth Syst. Sci. Data* **2020**, *12*, 847–867. [[CrossRef](#)]
71. Hansen, M.C.; Potapov, P.; Tyukavina, A. Comment on “Tropical forests are a net carbon source based on aboveground measurements of gain and loss”. *Science* **2019**, *363*, eaar3629. [[CrossRef](#)] [[PubMed](#)]
72. Hoesly, R.M.; Smith, S.J.; Feng, L.; Klimont, Z.; Janssens-Maenhout, G.; Pitkanen, T.; Seibert, J.J.; Vu, L.; Andres, R.J.; Bolt, R.M.; et al. Historical (1750–2014) anthropogenic emissions of reactive gases and aerosols from the Community Emissions Data System (CEDS). *Geosci. Model Dev.* **2018**, *11*, 369–408. [[CrossRef](#)]
73. Tyukavina, A.; Potapov, P.; Hansen, M.C.; Pickens, A.H.; Stehman, S.V.; Turubanova, S.; Parker, D.; Zalles, V.; Lima, A.; Kommareddy, I. Global trends of forest loss due to fire from 2001 to 2019. *Front. Remote Sens.* **2022**, *3*, 825190. [[CrossRef](#)]
74. Chang, X.; Xing, Y.; Wang, J.; Yang, H.; Gong, W. Effects of land use and cover change (LUCC) on terrestrial carbon stocks in China between 2000 and 2018. *Resour. Conserv. Recycl.* **2022**, *182*, 106333. [[CrossRef](#)]
75. Olofsson, P.; Foody, G.M.; Herold, M.; Stehman, S.V.; Woodcock, C.E.; Wulder, M.A. Good practices for estimating area and assessing accuracy of land change. *Remote Sens. Environ.* **2014**, *148*, 42–57. [[CrossRef](#)]
76. Zhao, T.; Zhang, X.; Gao, Y.; Mi, J.; Liu, W.; Wang, J.; Jiang, M.; Liu, L. Assessing the Accuracy and Consistency of Six Fine-Resolution Global Land Cover Products Using a Novel Stratified Random Sampling Validation Dataset. *Remote Sens.* **2023**, *15*, 2285. [[CrossRef](#)]
77. Li, Y.; Brando, P.M.; Morton, D.C.; Lawrence, D.M.; Yang, H.; Randerson, J.T. Deforestation-induced climate change reduces carbon storage in remaining tropical forests. *Nat. Commun.* **2022**, *13*, 1964. [[CrossRef](#)]

**Disclaimer/Publisher's Note:** The statements, opinions and data contained in all publications are solely those of the individual author(s) and contributor(s) and not of MDPI and/or the editor(s). MDPI and/or the editor(s) disclaim responsibility for any injury to people or property resulting from any ideas, methods, instructions or products referred to in the content.